Available online at www.sciencedirect.com
SCIENCE DIRECT®
Polymer 44 (2003) 3649–3660
polymer
www.elsevier.com/locate/polymer

Quantitative calculation of the orientation angles of adsorbed polyamides nanofilms

Tamara Elzein*, Maurice Brogly, Jacques Schultz

Institut de Chimie des Surfaces et Interfaces-CNRS, 15, rue Jean Starcky, 68057 Mulhouse, France

Received 27 January 2003; received in revised form 18 March 2003; accepted 2 April 2003

Abstract

Polyamides (PA) PA66, 610 and 612 were adsorbed as thin films on functionalized substrates. The conformational changes after adsorption are studied. New conformations due to the rotation of diamine/diacid planes were evidenced by infrared reflection absorption spectroscopy (IRRAS) and polarization modulation IRRAS (PM-IRRAS). The study of some infrared vibrators, which have a well defined transition moment direction with respect to the principal chain axis, allows us to access a qualitative information on the molecular orientation of PA chains. In this paper, we will discuss the possibility to obtain quantitative data on polyamide conformations on the basis of PM-IRRAS experiments. Values of orientation angles of diamine/diacid planes versus surface plane were determined. Similar angles are found in the four cases of gold, OH, NH_2 and COOH functionalized substrates, and for the three PA. Twist angle of about 20° is found between diamine and diacid planes. The chain orientation angles and conformations obtained do not depend on the substrate functionality and thus suggest that they are only the consequence of an adsorption effect.

Keywords: Orientation; PM-IRRAS; Nanofilms

1. Introduction

Interfacial characterization is of great interest for the understanding of the polymer adsorption in terms of chain orientation and conformation [1–7]. The creation of surfaces with specific applications could be done by adsorbing molecules with preferential orientation and, in some cases, different conformations relative to the bulk. In a recent work [8], we have showed that adsorbed polyamides (PA) PA66, 610 and 612, does not preserve their bulk conformations (Scheme 1). A twisted conformation between the diacid/diamine planes, initiated by adsorption, was evidenced. The quantitative calculation of these inter-planes orientation angles becomes possible by polarization modulation infrared reflection absorption spectroscopy (PM-IRRAS).

In this work we will discuss PM-IRRAS results and calculated values of orientation angles of PA66, 610 and 612 adsorbed on gold, and OH, NH_2 and COOH functionalized gold substrates.

2. Experimental section

2.1. Materials

The three PA were purchased from SIGMA ALDRICH Co. as 2–5 mm pellets. These PA are characterized by their T_g, T_f, T_B, and X_c, respectively, the glass transition temperature, melting and Brill temperatures and the degree of crystallinity [8]. Trichloroethanol (TCE) 99%, purchased from SIGMA ALDRICH, a common solvent of these three PA was used for the preparation of polyamide solutions (5 g/l). Thin films of PA were spin coated from solutions, with an acceleration of 10^3 rpm/s, a velocity of 2500 rpm and during 60 s, on the chosen substrates.

For sample preparation, the detailed procedure was extensively described in a previous study [8].

Gold coated substrates were prepared by using glass slides cleaned with ethanol, and treated by Argon plasma for 3 min at a power of 80 W. 3-Mercaptopropyltriethoxysilane

* Corresponding author. Tel.: +33-3-89-60-87-78; fax: +33-3-89-60-87-99.
E-mail address: tamara_elzein@yahoo.fr (T. Elzein).

0032-3861/03/$ - see front matter © 2003 Elsevier Science Ltd. All rights reserved.
doi:10.1016/S0032-3861(03)00293-3

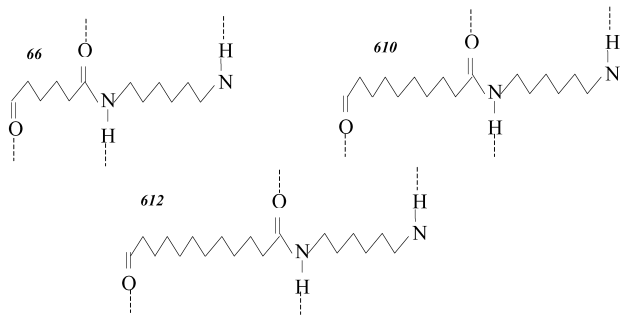

Scheme 1. Representation of bulk PA66, 610 and 612 linear chains.

(95%) from ABCR is then used as a coupling agent between glass slides and gold coatings. A 120 nm gold (99.99% from BALZERS) layer was then coated under vacuum of 10^{-7} mbar.

For grafting (e.g. Scheme 2), gold-coated substrates are then cleaned by UV radiation before being immersed in the grafts solution. The molecules used for the substrate functionalization are the following.

OH grafts: 11-mercapto-1-undecanol (97% from SIGMA ALDRICH) solution (in ethanol).
NH_2 grafts: 4-aminothiophenol (90% from SIGMA ALDRICH) solution (in ethanol).
COOH grafts: thioglycolic acid (99% from SIGMA ALDRICH) solution (in water).

Typical concentrations of 3 mM were used and immersion time was fixed to 12 h. Under these conditions, we obtain fully covered surfaces by the grafts self assembled monolayers [9].

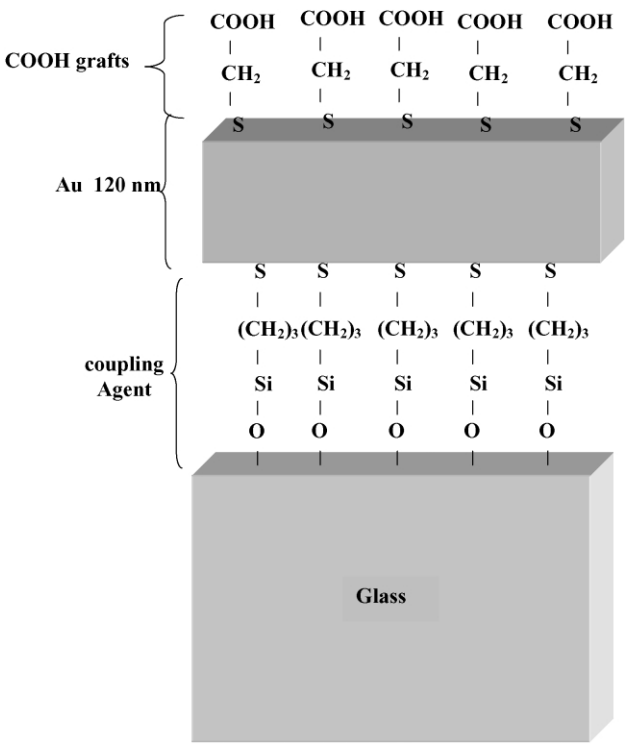

Scheme 2. Representation of COOH functionalized gold substrates.

2.2. Ellipsometry

Ellipsometric analyses were performed with an Optrel GdBR Multiskop in order to determine thin films thickness. Measurements were conducted on thin films coated on gold substrates using a laser beam having 532 nm, 0.6 mm, and 20 mW, respectively, for wavelength, diameter and intensity. Data evaluation is done with Elli program developed by Optrel GdBR as a part of the ellipsometry module of the Multiskop. Estimated thickness for the three PA samples are ranging from 42.4 to 42.8 nm.

2.3. Infrared spectroscopy

2.3.1. Attenuated total reflection (ATR)

Bulk PA were analyzed by single-reflection attenuated total reflection (ATR) spectroscopy. Measurements on PA pellets were performed with an IF66S Bruker spectrometer, a diamond crystal is used and the incidence angle of the beam is fixed to 45°. Spectra were recorded with a mercury-cadmium-telluride (MCT) detector. The number of scans was fixed to 100 with a resolution of 4 cm^{-1}.

2.3.2. Infrared reflection–absorption spectroscopy (IRRAS)

Thin films of PA adsorbed onto inert and functionalized gold substrates, were analyzed by infrared reflection-absorption spectroscopy (IRRAS). Measurements were done with an IFS66 Bruker spectrometer. Spectra recorded with a MCT detector were averaged over 500 scans, at a resolution of 1 cm^{-1}. The angle of the p polarized incident beam was fixed at 80°.

2.3.3. Polarization-modulation IRRAS (PM-IRRAS)

PM-IRRAS is highly dedicated to nanofilm analysis. Classical IRRAS experiments consist in recording the p-polarized reflectivity $R_p(d)$ and for ultra thin films, the surface detectivity of IRRAS is not sufficient and very long measurement times became necessary. These limitations are resolved by 'coding' the surface with some kind of modulation technique. Thus in PM-IRRAS (Scheme 3) a differential reflectivity ($\Delta R/R$) surface signal is obtained in one step and with all the dynamical range of the detection [10]. It is important to remember that this technique is based on three principles.

- The selection rules induced by the reflection of an infrared beam under p polarization and grazing angles on metallic surface: when a dipole moment is oriented in the surface normal direction, its signal is intensified in the PM-IRRAS spectrum.
- The double modulation of the incident beam.

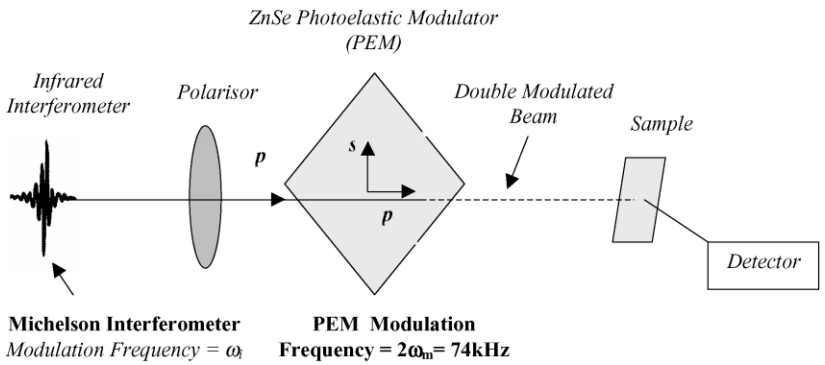

Scheme 3. Optical PM-IRRAS setup.

- The mathematical treatment of the detected signal that allows to obtain the differential reflectivity.

So, compared to the IRRAS method, PM-IRRAS presents at least two decisive advantages of a much higher surface absorption sensitivity and of the in situ experimental ability, while it still conserves the IRRAS advantages of electric field enhancement and the surface selection rules. Conversely, the experimental setup, the procedure and the quantitative analysis treatments becomes more complex [10].

Measurements were done with an IF66S Bruker spectrometer, spectra recorded with MCT detector, under experimental conditions of 1000 scans, resolution of 1 cm^{-1}, 85° as beam incidence angle and with a 74 kHz modulation frequency. A ZnSe photoelastic modulator provided by HINDS™ is used.

PM-IRRAS technique allows no environmental perturbation on the spectra and high signal to noise ratio. A background spectrum is typically taken to eliminate any instrumental artifacts.

For the spectral decomposition of overlapped bands into individual bands we used the second derivative method performed with the OPUS® software supplied by the spectrometer manufacturer. This software gives also, for each fit, the calculation error which is minimized.

We used the second derivative method to determine the number and the frequency of overlapped bands. Sharp bands are fitted with a pure Lorentzian function, while large ones are a combination of Lorentzian and Gaussian functions. This latter is the consequence of the multiple Lorentzian components summation.

3. Results and discussion

The results will be discussed in two parts: qualitative results and quantitative orientation determination.

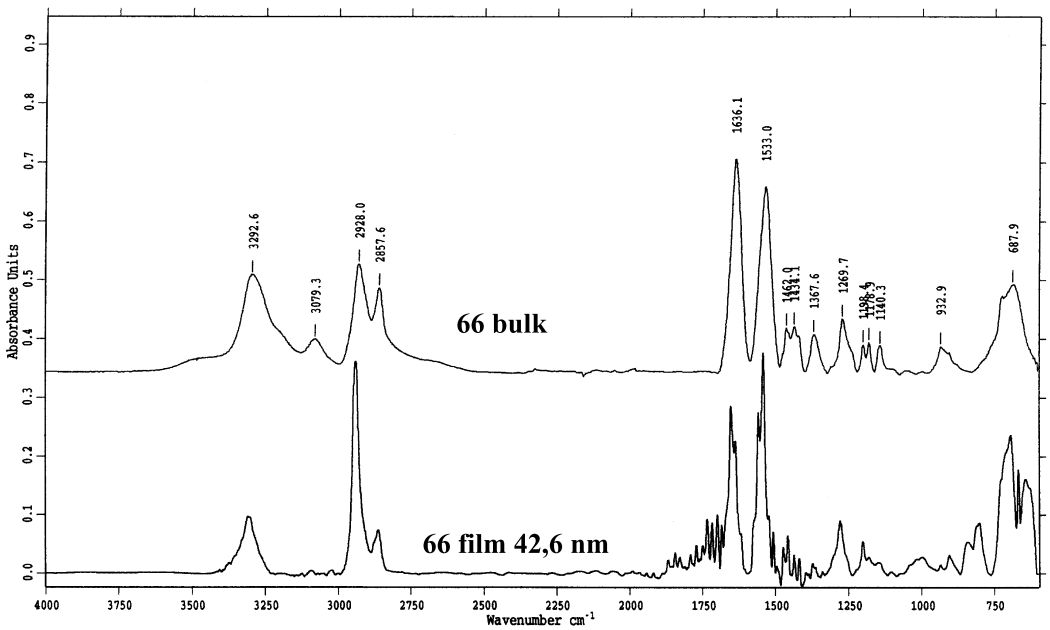

Fig. 1. ATR spectra of bulk PA 66 compared with IRRAS spectra of 33 nm thin film adsorbed on gold substrate.

Table 1
Characteristics of PA infrared vibrators

Vibrator	Position (cm^{-1})	Attribution [11–14]
Amide V: deformation γ(NH)	690	α and β plane forms
	710	γ non-plane form
Stretching ν(N–C=O)	900–907	Triclinic structure
Rocking r(NH)	983–987	Triclinic structure
Skeletal stretching ν(C–C)	1014–1019, 1033–1043, 1063–1066	Triclinic structure
Twisting t(CH_2) coupled with amide	1224–1228	Triclinic structure
Twisting t(NH)	1300–1305	Triclinic structure
Wagging w(CH_2) coupled with amide	1329	Triclinic structure
Stretching ν(C–N) + bending δ(NH)	1540	α and β plane forms
	1560	γ non-plane form

3.1. Qualitative results

This part concerns the vibrational study of adsorbed PA compared to the bulk isotropic state. In order to understand the variation of spectral response induced by adsorption.

A comparison between bulk (ATR) and thin film (IRRAS) spectra of PA 66 is shown in Fig. 1. Adsorbed film thickness is 42.6 nm.

Five regions of interest appear in these spectra.

- The amide IV, V, VI regions (600–800 cm^{-1}),
- the triclinic cell region (900–1300 cm^{-1}),
- the amide I and amide II regions (1500–1700 cm^{-1}),
- the CH_2 stretching mode region (2700–3000 cm^{-1}),
- the NH stretching mode region (3000–3500 cm^{-1}).

For the four types of substrates (inert and functionalized), the triclinic structure of PA in thin films is confirmed by the fact that the amide II band is centered at 1544 cm^{-1}, and by the presence of bands at 906, 985, 1015, 1066, 1228, and 1305 cm^{-1} that are characteristics of the triclinic cell [11–14]. These bands assignments are gathered in Table 1.

3.1.1. Bulk and thin films comparisons

To avoid environmental perturbations in our comparisons, we choose to work with PM-IRRAS spectra that presents a better signal to noise ratio and which offers direct and quantitative comparison.

3.1.1.1. Amide I and Amide II region (1500–1800 cm^{-1}). Comparison of bulk and thin film spectra is shown in Fig. 2. The existence of strong amide I band indicates that C=O transition moments interact with the electric field vector of the incident beam. Therefore the C=O groups are suspected to be preferentially oriented in the normal direction with respect to the substrate plane. In the case of these PA, the C=O groups are almost oriented perpendicular to the chain main axis, due to the stabilization of *trans–trans* extended conformations of the chains by quite perpendicular inter-chain H-bonds. As a consequence, parallel orientation of the chains with respect to the interface will induce a quite perpendicular orientation of the C=O groups.

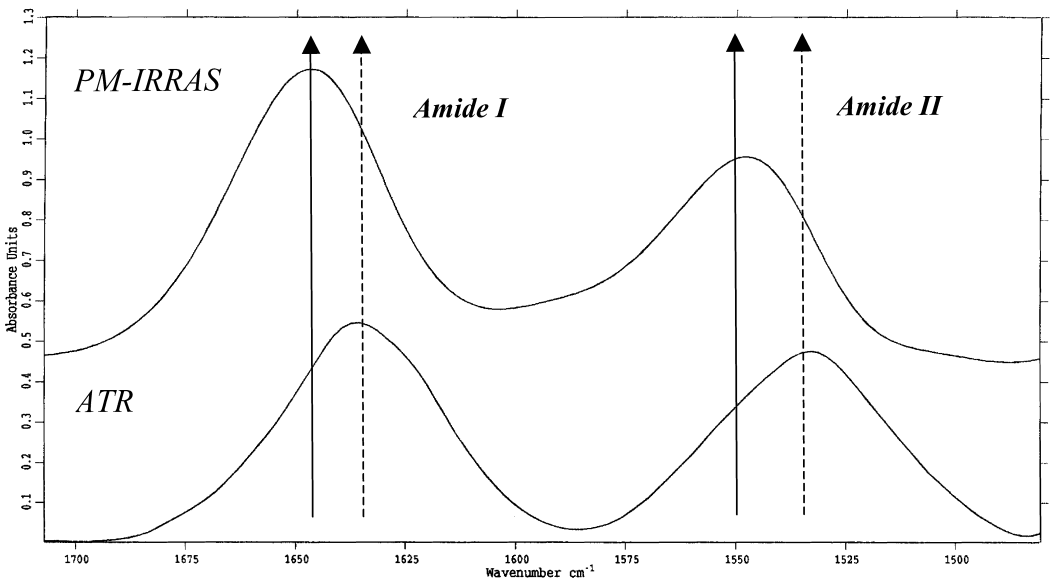

Fig. 2. Comparison of PA66 bulk ATR spectrum and PA66 thin film PM-IRRAS spectrum, on NH_2 substrates, in the 1500–1800 cm^{-1} region.

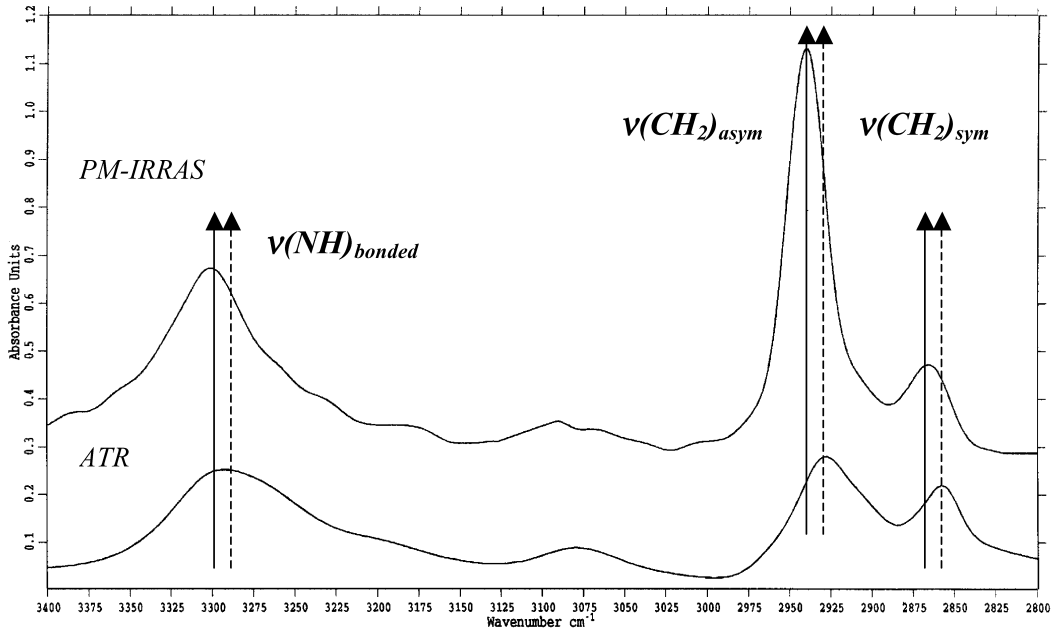

Fig. 3. Comparison of PA66 bulk ATR spectrum and PA66 thin film PM-IRRAS spectrum, on COOH substrates, in the 2800–3500 cm^{-1} region.

Frequencies shifts and shapes changes are induced by the geometric differences of ATR and PM-IRRAS, and by thin films selection rules of this latter. Moreover, the composition of these two bands may change after adsorption due to these selection rules that enhance some components comparing to others.

3.1.1.2. The NH stretching mode region (3000–3500 cm^{-1}). The presence of NH stretching modes (Figs. 1 and 3) of species involved in hydrogen bonds (3000–3500 cm^{-1}) is observed. This fact supports the existence of C=O stretching modes at 1600–1700 cm^{-1}, since hydrogen bonds are established between the C=O and NH groups. As a consequence, transition moments, in the special case of intra or inter chains H-bonds, must be in the same orientation.

In Fig. 3, we could observe frequency and intensity changes. The frequency shift, as noticed already, is a geometric consequence, while intensity changes are directly related to the vibrator orientation and to the amount of crystalline phase. These great changes in the CH_2 stretching region would be very useful for the orientation determination. On the other hand, the bonded NH stretching modes could be also very interesting vibrators for crystallinity estimation.

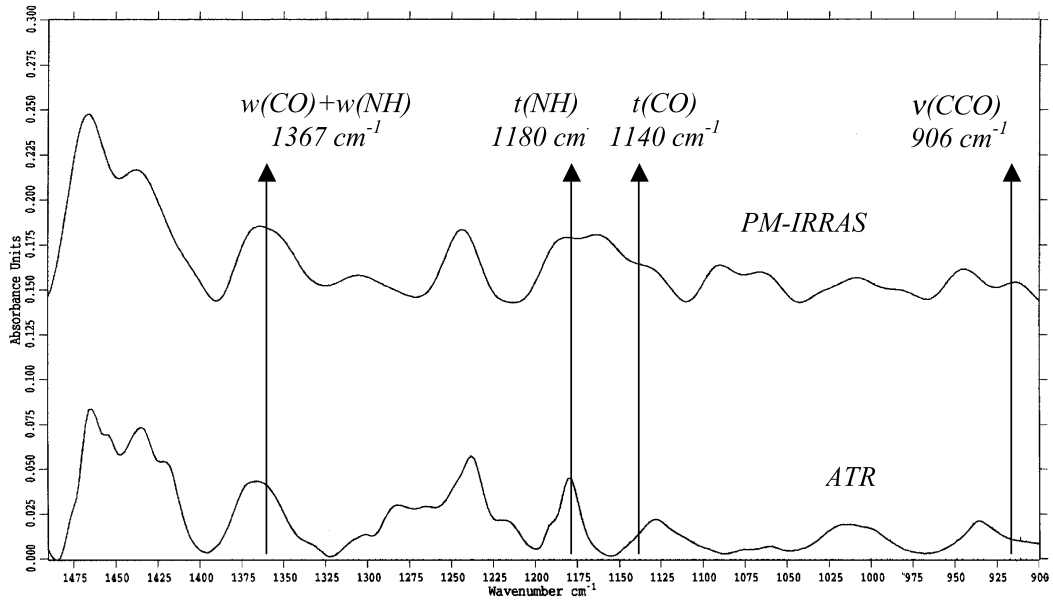

Fig. 4. Comparison of PA610 bulk ATR spectrum and PA610 thin film PM-IRRAS spectrum, on OH substrates, in the 900–1500 cm^{-1} region.

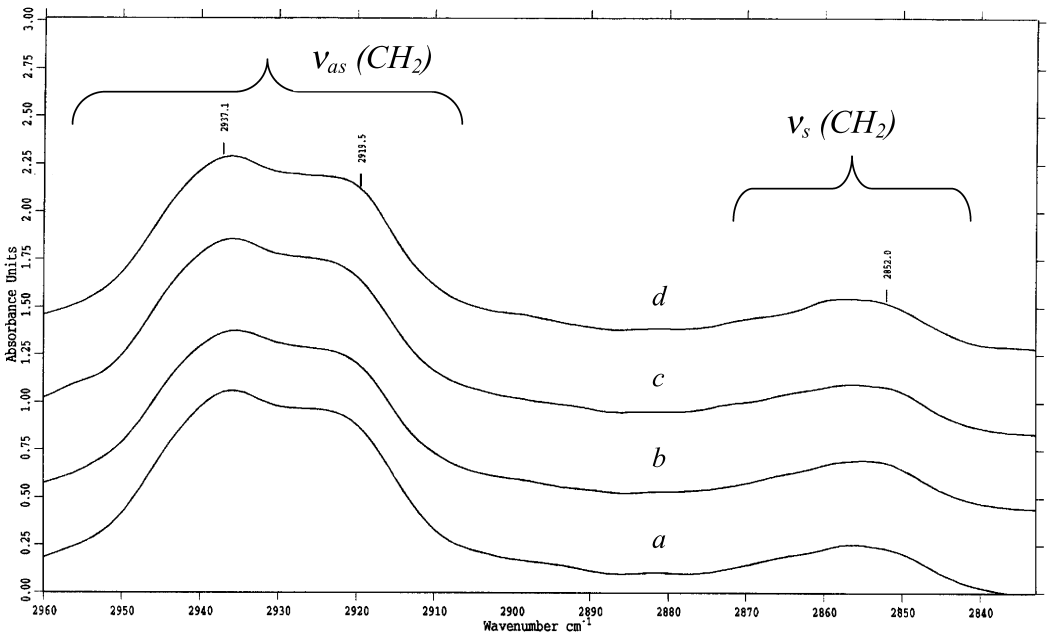

Fig. 5. Comparison of PA612 PM-IRRAS spectra on: (a) Inert, (b) NH_2, (c) COOH, and (d) OH substrates.

3.1.1.3. The 600–1500 cm^{-1} region. Comparison of bulk and thin films spectra (Fig. 4) reveals also differences for bands such as: rocking r(NH) and rocking r(C=O) at 600–900 cm^{-1}, stretching ν(C–C=O) at 906 cm^{-1}. Moreover intensity changes of twisting t(C=O), t(NH) at 1140 and 1180 cm^{-1}, and wagging w(C=O) coupled with w(NH) at 1367 cm^{-1} are observed.

We should mention the difficulty we have to interpret intensity changes in this region. In fact, many bands are overlapped and the resulting spectrum is complex. Nevertheless, strong bands, that already contribute to the crystalline structural identification, could be useful for the understanding of chain orientation, as it would be discussed later in the paper.

Table 2
Vibrators modes and their direction with respect to the chain plane and to the middle axis of C–C–C

Modes	Range (cm^{-1})	Transition moment direction [15–17]
r(NH) + r(C=O)	600–900	In the chain plane, quite perpendicular to the chain axis
ν(C–C=O)	906	In the chain plane, quite perpendicular to the chain axis
t(C=O)	1140	Perpendicular to the chain plane and to the chain axis
t(NH)	1180	Perpendicular to the chain plane and to the chain axis
w(C=O) + w(NH)	1367	Perpendicular to the chain plane and to the chain axis
ν(CN) + δ(NH)	1500–1580	In the chain plane, quite perpendicular to the chain axis
ν(C=O)	1600–1690	In the chain plane, perpendicular to the chain axis
$\nu_s(CH_2)$	2840–2870	In the chain plane, perpendicular to the chain axis
$\nu_{as}(CH_2)$	2910–2950	Perpendicular to the chain plane and to the chain axis
ν(NH)	3000–3400	In the chain plane, perpendicular to the chain axis

3.1.1.4. CH_2 stretching mode regions (2800–3000 cm^{-1}). Important differences are observed in the asymmetric CH_2 stretching mode (Figs. 1 and 3), and a closer observation (Fig. 5) shows a splitting of the $\nu_{as}(CH_2)$ in two contributions. The first one, located at 2938 cm^{-1} is attributed to the diamine CH_2 groups, and the second one, located at 2920 cm^{-1}, is related to the diacid CH_2 entities. Detailed explanation of these two components has already been proposed [8], where we consider that, the linear increase of the second component intensity with the diacid aliphatic carbons number, implies a twist of the diamine/diacid planes.

Unpredicted results about the chemical functionality effect is experimentally observed (Fig. 5). It appears that lateral grafts–grafts and polymer–polymer interactions dominate the polymer–grafts ones, and thus no great differences are observed between the four substrates. This hypothesis would be examined by studying the grafting density effect on PA chain orientation.

The combination of these observations with the examination of all vibrators moment direction (gathered in Table 2) permits to propose a model (Scheme 4) in which a rotation of the diacid/diamine planes is present for PA chains adsorbed in thin films.

Taking into account the sensibility of this technique toward the specific orientation, we can qualitatively justify the enhancement or the decrease of PM-IRRAS bands intensities according to Table 2 on the basis of Scheme 4.

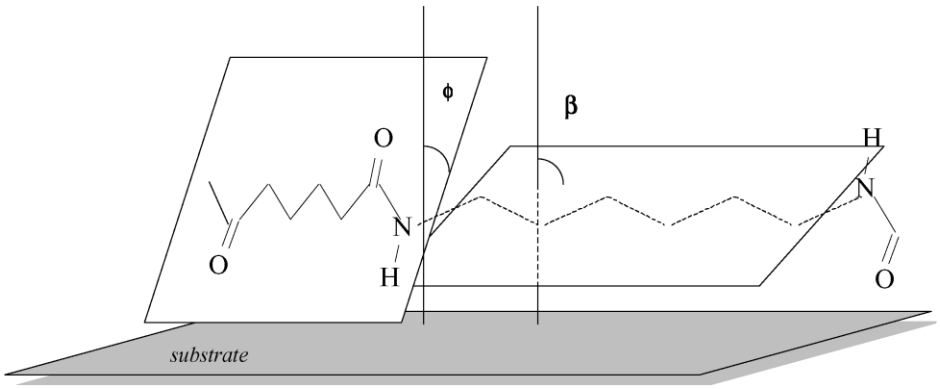

Scheme 4. Proposed model for chain conformation of adsorbed PA.

3.2. Orientation determination

3.2.1. PM-IRRAS theory

At grazing angle of incidence, the intensity of a reflected p-polarized infrared light beam is enhanced at a metal surface [18,19]. This polarization leads to strong selection rules at the surface and has been used to deduce information of adsorbed polymers such as molecular orientation [20–30].

In addition to orientation measurements, the predominance of p-polarized light over s-polarized light at the metal surface has been used to obtain the differential reflectance spectrum of the adsorbed surface species, $\Delta R/R$, by polarization modulation of the infrared light [31–40] (modulation frequency of 74 kHz).

In order to analyze precisely the IR response of a three phase system (namely air (1)–polymer thin film (2)–substrate(3)) one has to establish the infrared PM-IRRAS selection rules, in the case of thin film approximation. Of course we have to take into account the specific orientation of IR vibrators in an expected IR intensity. The expression of the IR detected signal, in a PM-IRRAS experiment on a metallic substrate, is given by the following expression

$$S(d) = \frac{[R^{P}_{123}(\nu) - R^{S}_{123}(\nu)]J_2(\phi_1)}{[R^{P}_{123}(\nu) + R^{S}_{123}(\nu)]} \tag{1}$$

where R is the reflectivity of a three phase system, superscripts S and P refer to the polarization state of the incident IR wave, respectively, parallel (P) and perpendicular (S). ν is the IR wavenumber and J_2 is the second order Bessel function.

If we expect that specific orientation occurs in the adsorbed thin film, the orientation of transition moments has an influence on the resulting IR reflectivity. In the case of an uniaxialy oriented film we define q as the angle between a transition moment M and the Oz axis normal to the surface plane. Then, the polymer film (medium 2) is characterized by a complex refractive index equal to $\hat{n}_{2xy} = n_2 - ik_{2xy}$ in the Oxy surface plane, and $\hat{n}_{2z} = n_2 - ik_{2z}$ in Oz direction (normal to the surface plane), where the absorption index k is defined as

$$k = \frac{1}{3}(k_x + k_y + k_z), \qquad k_x = k_y = \frac{3}{2}k\sin^2\theta,$$
$$k_z = 3k\cos^2\theta \tag{2}$$

If for each i phase of the 3-phase system we define a Fresnel term as, $\xi_i = \hat{n}_i \cos\theta_i$ then the complex reflectivities between two phases i and j are given for P and S polarization states by

$$\hat{r}^{P}_{ij} = \frac{\hat{\epsilon}_j\xi_i - \hat{\epsilon}_i\xi_j}{\hat{\epsilon}_j\xi_i + \hat{\epsilon}_i\xi_j} \quad \text{and} \quad \hat{r}^{S}_{ij} = \frac{\xi_i - \xi_j}{\xi_i + \xi_j}$$

$\hat{\epsilon}_i$ and $\hat{\epsilon}_j$ are the dielectric constants of medium i and j. These latter depend on the complex refractive index according to

$$\hat{\epsilon}_i = \epsilon'_i - i\epsilon''_i \qquad \epsilon'_i = n_i^2(\nu) - k_i^2(\nu)$$
$$\epsilon''_i = 2n_i(\nu)k_i(\nu) \tag{3}$$

finally the complex reflectivity for the 3-phase interface is

$$\hat{r}^{P,S}_{123}(\nu) = \frac{\hat{r}^{P,S}_{12}(\nu) + \hat{r}^{P,S}_{23}(\nu)\exp\left(\frac{-i4\pi\hat{n}_2(\nu)d\cos\theta_2}{\lambda}\right)}{1 + \hat{r}^{P,S}_{12}(\nu)\hat{r}^{P,S}_{23}(\nu)\exp\left(\frac{-i4\pi\hat{n}_2(\nu)d\cos\theta_2}{\lambda}\right)} \tag{4}$$

Where λ is the wavelength. The detected reflectivity as measured in Eq. (1) is then: $R^{P,S}_{123}(\nu) = \hat{r}^{P,S}_{123}(\nu)\cdot\hat{r}^{P,S^*}_{123}(\nu)$

We are now able to establish the PM-IRRAS selection rules i.e. the sign and intensity of an IR band as a function of the orientation of a transition moment (or functional group) relative to the surface plane. Selection rules are then: if the orientation of a transition moment is parallel to the surface plane then the PM-IRRAS signal is equal to zero. If the orientation is perpendicular to the surface plane then the signal is maximum.

3.2.2. Application for PA thin films

For quantitative calculations it is important to choose appropriate vibrators. In our case, interesting vibrators, with high intensity and composed of single mode without overlapping, are the H-bonded NH stretching modes

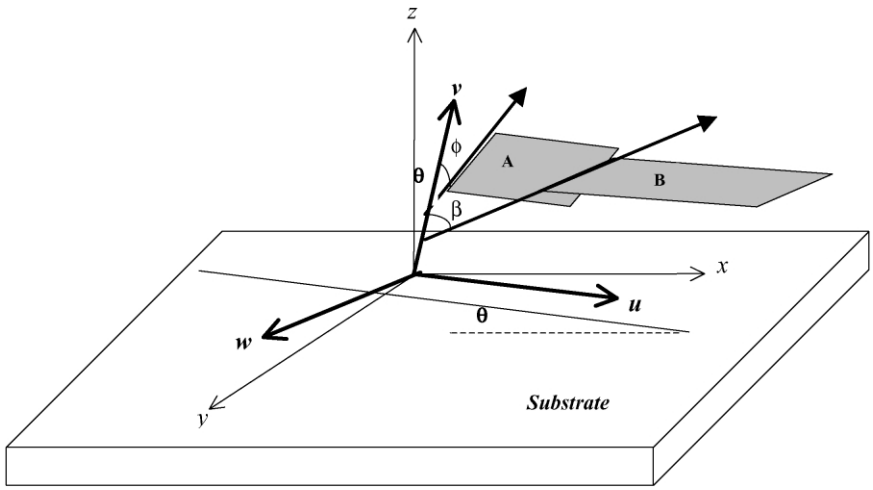

Scheme 5. Representation of the PA chains in the *u*, *v*, *w* and *x*, *y*, *z* referentials.

(3000–3400 cm^{-1}) and the CH_2 asymmetric stretching modes (2900–2970 cm^{-1}). These latter are sensitive to the diacid and diamine planes, since that its two components could be easily decomposed in the PM-IRRAS spectra.

In Scheme 5, we have represented the A and B planes relative, respectively, to the diacid and diamine planes. We would suppose that PA coordinates are expressed in the *u*, *v*, *w* referential. The *u*, *v*, *w* referential is related to the substrate *x*, *y*, *z* referential by the angle θ (angle formed between the chain axis and the substrate plane). According to this scheme, the projection of the chain main axis is in the *u* direction. The diacid and diamine planes are related to the *v* axis, respectively, by ϕ and β.

In Scheme 6, we have represented the $\nu(NH)_b$, $\nu s(CH_2)_{diacid}$, $\nu as(CH_2)_{diacid}$, $\nu s(CH_2)_{diamine}$, $\nu as(CH_2)_{diamine}$ transition moments, that correspond, respectively, to the bonded NH stretching modes, CH_2 symmetric and asymmetric modes of the diacid and diamine planes, with respect to *v* axis.

3.2.3. Principle

According to PM-IRRAS rules [41,42], the interfacial IR reflectivity is expressed as

$$I_i \propto [F_i(\theta, \phi, \beta\ldots)]^2 A_i$$

where I_i is the PM-IRRAS experimental integrated intensity of a given thin filmband, F_i represents a geometric function that depends on the vibrator direction in the referential, and A_i is the bulk isotropic state integrated intensity. By taking two transition moments *i* and *j* we deduce

$$I_i/I_j = [F_i(\theta,\phi,\beta\ldots)]^2 A_i / [F_j(\theta,\phi,\beta\ldots)]^2 \cdot A_j \quad (5)$$

The geometric function *F* of the chosen vibrators are listed in Table 3.

It is important to note that in this case: ϕ, average angle between diacid and *v* axis, $\phi = (\nu(NH)_{bonded}, v) = (\nu s(CH_2)_{diacid}, v)$; β, average angle between diamine and *v* axis, $\beta = (\nu s(CH_2)_{diamine}, v)$.

By replacing *F* in the equations of chosen vibrators, we obtain

$$I(NH)_b \propto (\cos\theta \cos\phi)^2 A(NH)_b \quad (6)$$

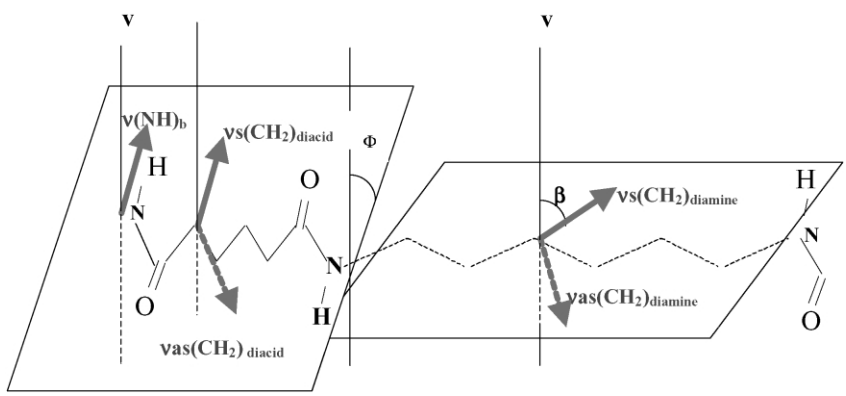

Scheme 6. Representation of transition moments according to the proposed model.

Table 3
Transition moment directions and the corresponding geometric function F

Vibration mode	Wavenumber ν (cm^{-1})	Transition moment vector M	Direction in u, v, w referential	Geometric function F
$\nu(NH)_b$	300–3400	In the diacid plane ⊥ to the main chain axis	In the (u,v) plane $-\cos\phi$	$\cos\phi\cdot\cos\theta$
$\nu as(CH_2)_{diamine}$	≈2936	⊥ to the diamine plane ⊥ to the main chain axis	In the (u,v) plane $-\sin\beta$	$\sin\beta\cdot\cos\theta$
$\nu as(CH_2)_{diacid}$	≈2920	⊥ to the diacid plane ⊥ to the main chain axis	In the (u,v) plane $-\sin\phi$	$\sin\phi\cdot\cos\theta$

Table 4
Values of K and K'

	PA66	PA610	PA612
K	4/10	8/14	10/16
K'	6/10	6/14	6/16

$$I(CH_2)as_{diacid} \propto [\cos\theta\cos(90-\phi)]^2 A(CH_2)as_{diacid}$$
$$\propto (\cos\theta\sin\phi)^2 A(CH_2)as\cdot K \quad (7)$$

$$I(CH_2)as_{diamine} \propto [\cos\theta\cos(90-\beta)]^2 A(CH_2)as_{diamine}$$
$$\propto (\cos\theta\sin\beta)^2 A(CH_2)as\cdot K' \quad (8)$$

K and K' are constants relating, respectively, the diacid and the diamine integrated intensity to the total methylene absorption intensity experimentally obtained in the case of bulk sample. Since that their responses in linear chains are obtained at the same frequency, we consider that the response of diacid or diamine part is proportional to the ratio of its aliphatic methylene groups. As an example, in PA66, the diacid part contain four aliphatic methylene groups whereas the diamine one contain six aliphatic methylene. Thus, for PA66, $K = 4/(4+6)$ and $K' = 6/(4+6)$. Values of K and K' are gathered in Table 4.

The combination of Eqs. (6)–(8) permits to obtain ϕ and β. This can be done if the values of $I(NH)_b$, $I(CH_2)as_{diacid}$, and $I(CH_2)as_{diamine}$ are known.

The first term is obtained by integration of each spectrum, between 3000 and 3400 cm^{-1}.

For the two other terms, an example of spectral decomposition is shown in Fig. 6.

The integrated intensities of these two components are obtained after curve fitting.

3.2.4. Calculations

By combining Eqs. (6) and (7) we obtain

$$\frac{I(CH_2)as_{diacid}}{I(NH)_b} = \left(\frac{\sin\phi}{\cos\phi}\right)^2 \frac{A(CH_2)as}{A(NH)b} K \quad (9)$$

and thus

$$tg\phi = \sqrt{\frac{I(CH_2)as_{diacid} A(NH)_b}{I(NH)_b A(CH_2)as\cdot K}} \quad (10)$$

On the other hand, Eqs. (7) and (8) give relation Eq. (11)

$$\frac{I(CH_2)as_{diamine}}{I(CH_2)as_{diacid}} = \left(\frac{\sin\beta}{\sin\phi}\right)^2 \frac{A(CH_2)as\cdot K'}{A(CH_2)as\cdot K} \quad (11)$$

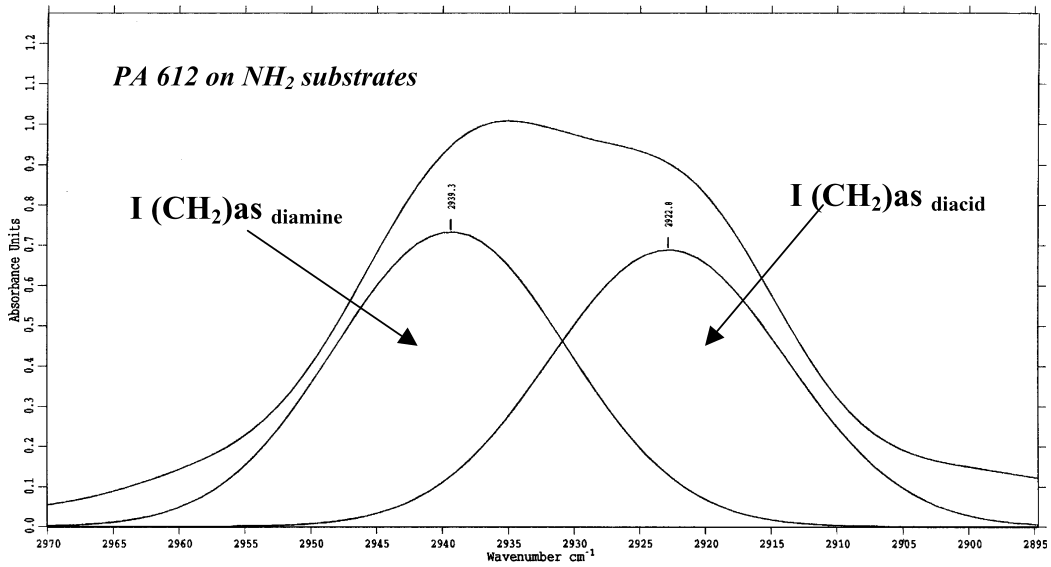

Fig. 6. Spectral decomposition of a PA612 PM-IRRAS spectrum in the 2895–2960 cm^{-1} region.

Table 5
Calculated values of ϕ

ϕ (°)	Gold substrates	NH_2 substrates	COOH substrates	OH substrates
PA66	40	41	40	41
PA610	41	43	44	42
PA612	43	43	40	41

Table 6
Calculated values of β

β (°)	Gold substrates	NH_2 substrates	COOH substrates	OH substrates
PA66	62	62	62	63
PA610	62	62	63	62
PA612	64	63	60	63

Table 7
Calculated values of the twist angle between the diamine and diacid planes

$\beta-\phi$ (°)	Gold substrates	NH_2 substrates	COOH substrates	OH substrates
PA66	22	21	21	22
PA610	21	19	19	20
PA612	21	20	20	22

that gives

$$\sin\beta = \frac{\sin\phi}{\sqrt{\dfrac{I(CH_2)as_{diacid}K'}{I(CH_2)as_{diamine}K}}} \quad (12)$$

By replacing all measured values from infrared spectra in Eqs. (10) and (12), we access to the determination of ϕ and β for each PA adsorbed on the four types of substrates, as listed in Tables 5 and 6.

The values of the twist angle ($\beta-\phi$) are listed in Table 7.

As we can see, for each PA, no significant differences are observed due to changes in the surface functionality (Tables 5–7 and Figs. 7 and 8). This evidence leads us to consider that the preferential orientation of PA66, 610 and 612 is independent of the surface chemistry. We could also

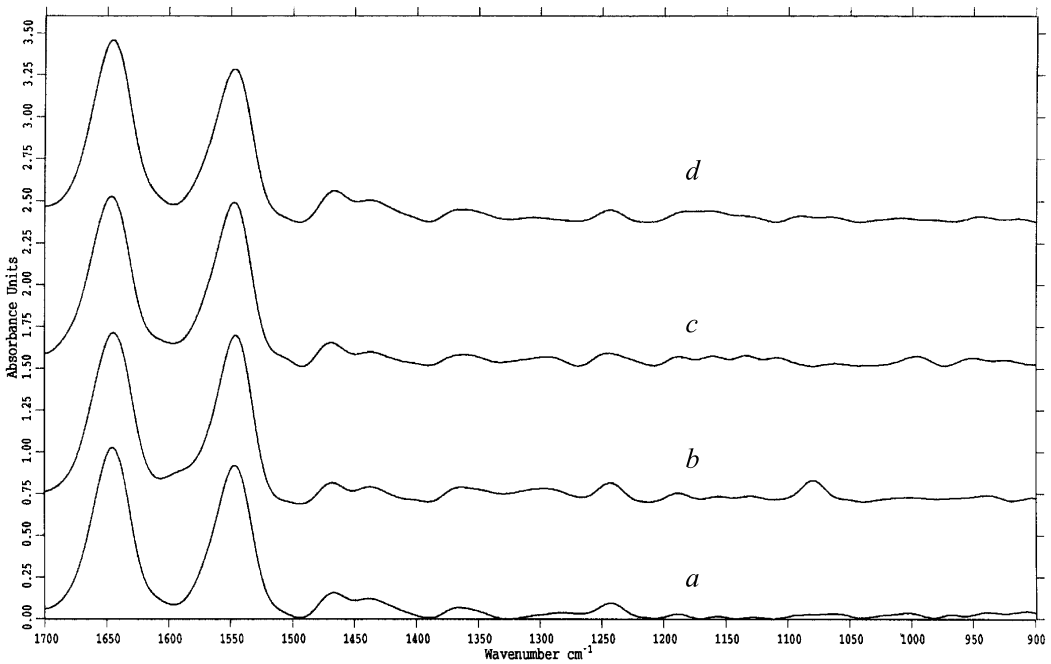

Fig. 7. Comparison of PA610 PM-IRRAS spectra: (a) Inert, (b) NH_2, (c) COOH, and (d) OH substrates, in the 900–1800 cm^{-1} region.

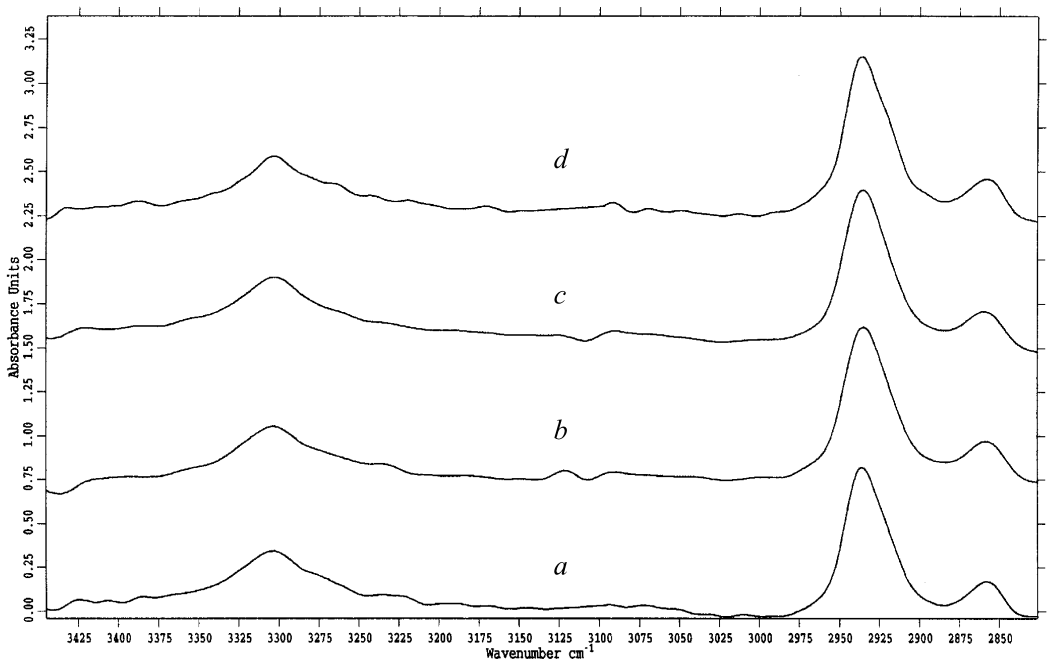

Fig. 8. Comparison of PA610 PM-IRRAS spectra: (a) Inert, (b) NH_2, (c) COOH, and (d) OH substrates, in the 2800–3500 cm^{-1} region.

consider that conformational changes is a consequence of adsorption and do not result from chain–grafts interactions. Indeed for gold inert substrates the same changes were observed without significant differences of angle values (Tables 5–7).

In fact, these results were not suspected, and a predominant functionality effect was expected. The experimental results were contradictory: the surface functionality seems to be inactive in terms of PA chains–grafts interaction: Acid–base interactions are to be expected at the interface vicinity between the PA chains (C=O and NH groups) and the surface functions (OH, NH_2, COOH). However, the fact that PA crystalline structures are stabilized by the inter-chain hydrogen bonds between the Polyamides CO and NH groups do not allow these latter to get involved in interfacial interactions with the surface. So, it seems that these interfacial interactions are absent, and even if we assume that some of them exist, they could not induce a driving force to reorient the PA chain in the thin film. It is also of major importance to argue in term of bonds energy: 46, 29 and 22 J mol^{-1} representing the enthalpy of, respectively, CO–NH interaction between PA chains, C=O–HO interaction between two COOH grafts and NH–NH interaction between two NH_2 grafts [43]. On the basis of these values, we could justify the non-detected interfacial interactions and thus the absence of direct incidence on the PA chains orientation.

4. Conclusion

In this work, we were interested in determining the orientation angles of PA66, 610 and 612 chains adsorbed on four types of surface: inert, NH_2, COOH and OH functionalized substrates. This calculation is made by using the PM-IRRAS technique adapted to thin films study and that offers quantitative spectral information.

This study improves the suitability of the PM-IRRAS technique to study orientation in thin films. Moreover, this technique allowed us to access to quantitative data and to elaborate a conformation model of PA chains adsorbed on chemically modified interfaces.

Experimental results shows a conformational change of linear PA chains, that are lying quite parallel to the interface, by comparison with the bulk state. The diacid plane of PA has a tilt angle of about 40° with respect to the substrate normal, while the diamine plane is twisted of about 20° with respect to the diacid one.

No great differences are observed when changing the surface chemistry due to the crystalline stabilization that involves important polymer chain–chain interactions. Thus, inter-chain hydrogen bonds between PA chains do not offer to CO and NH groups the possibility to get involved into acid-base interfacial interactions with the surface grafts.

References

[1] Jimbo T, Tanioka A, Minoura M. Langmuir 1999;15:1829.
[2] Han SW, Kim CH, Hong SH, Chung YK, Kim K. Langmuir 1999;15:1579.
[3] Hausch M, Beyer D, Knoll W, Zentel R. Langmuir 1998;14:7213.
[4] Caruso F, Furlong DN, Ariga K, Ichinose I, Kunitake T. Langmuir 1998;14:4559.
[5] Mao L, Ritcey AM, Desbat B. Langmuir 1996;12:4754.
[6] Worley CG, Linton RW, Samulski ET. Langmuir 1995;11:3805.
[7] Okamura E, Umemura J, Takenaka T. Can. J. Chem. 1991;69:1691.

[8] Elzein T, Brogly M, Castelein G, Schultz J. J. Polym. Sci. B 2002;40: 1464.
[9] Elzein T, Brogly M, Schultz J. J. Surf. Interface Anal. 2003;35:231.
[10] Buffeteau T, Desbat B, Turlet JM. Appl. Spectrosc. 1991;45:380.
[11] Hummel DO. Infra red spectra of polymers. New York: Wiley; 1966.
[12] Vasanthan N, Salem DR. J. Polym. Sci. B 2000;38:516.
[13] Vasanthan N, Murthy NS, Bray RG. Macromolecules 1998;31:8433.
[14] Koenig JL, Agboatwalla MC. J. Macromol. Sci. Phys. B 1968;2:39.
[15] Schrader B. Infrared and Raman spectroscopy, methods and applications. Wienheim: VCH; 1995.
[16] Brittain EFH, George WO, Wells CHJ. Introduction to molecular spectroscopy. New York: Academic Press; 1970.
[17] Colthup NB, Daly LH, Wiberley SE. Introduction to infrared and Raman spectroscopy, 3rd ed. London: Academic Press; 1990.
[18] Greenler RG. J. Chem. Phys. 1966;44:310.
[19] Greenler RG. J. Chem. Phys. 1969;50:1963.
[20] Rabolt JF, Burns FC, Schlotter NE, Swalen JD. J. Chem. Phys. 1983; 78:946.
[21] Gun J, Iscovici R, Sagiv J. J. Colloid Interfacial Sci. 1984;101:201.
[22] Swalen JD, Rabolt JF. Fourier Transform Infrared Spectrosc. 1985;4: 283.
[23] Allara DL, Nuzzo RG. Langmuir 1985;1:52.
[24] Schlotter NE, Porter MD, Bright TB, Allara DL. Chem. Phys. Lett. 1986;132:93.
[25] Gun J, Sagiv J. J. Colloid Interface Sci. 1986;112:457.
[26] Nuzzo RG, Fusco FA, Allara DL. J. Am. Chem. Soc. 1987;109:2358.
[27] Porter MD, Bright TB, Allara DL, Chidsey CED. J. Am. Chem. Soc. 1987;109:3559.
[28] Porter MD. Anal. Chem. 1988;60:1143A.
[29] Troughton EB, Bain CD, Whitesides GM, Nuzzo RG, Allara DL, Porter MD. Langmuir 1988;4:365.
[30] Yen YS, Wong JS. J. Phys. Chem. 1983;93:7208.
[31] Golden WG, Dunn DS, Overend J. J. Catal. 1981;71:395.
[32] Dowry AE, Marcott C. Appl. Spectrosc. 1982;36:414.
[33] Golden WG, Saperstein DD. J. Electron Spectrosc. Relat. Phenom. 1983;30:43.
[34] Golden WG, Saperstein DD, Severson MW, Overend J. J. Phys. Chem. 1984;88:572.
[35] Pang KP, Benziger JB, Soriaga MP, Hubbard AT. J. Phys. Chem. 1984;88:4583.
[36] Golden WG, Kunimatsu K, Seki H. J. Phys. Chem. 1984;88:1275.
[37] Golden WG. Fourier Transform Infrared Spectrosc. 1985;4:315.
[38] Kuminatsu K, Golden WG, Seki H, Philpott MR. Langmuir 1985;1: 245.
[39] Kuminatsu K, Samant M, Seki H, Philpott MR. J. Electroanal. Chem. Interfacial Electrochem. 1988;243:203.
[40] Barner BJ, Green MJ, Saez EI, Corn RM. Anal. Chem. 1991;63:55.
[41] Buffeteau T, Desbat B, Pézolet M, Turlet JM. J. Chim. Phys. 1993;90: 1467.
[42] Buffeteau T, Desbat B, Devaure J, Salimi A, Turlet JM. J. Chim. Phys. 1993;90:1871.
[43] Coleman MM, Graf JF, Painter PC. Specific interactions and the miscibility of polymer blends. USA: Technomic Publishers; 1991.